Sparse grid reconstructions for Particle-In-Cell methods

M. Chung-To-Sang[‡], F. Deluzet[†],G. Fubiani[‡] L. Garrigues [‡], C. Guillet[†‡], J. Narski[†]

[†] Institut de Mathématiques de Toulouse (IMT)
[‡] Laboratoire Plasma et Conversion d'énergie (LAPLACE)

May 18, 2022

Mathematical model

Vlasov-Poisson system:

$$\begin{cases} \dfrac{\partial f_s}{\partial t} + \mathbf{v} \cdot \nabla_{\mathbf{x}} f_s + \dfrac{q_s}{m_s}(\mathbf{E} + \mathbf{v} \times \mathbf{B}) \cdot \nabla_{\mathbf{v}} f_s = 0, \\ \nabla \cdot \mathbf{E} = \dfrac{\rho}{\varepsilon_0}, \qquad \mathbf{E} = -\nabla \Phi, \end{cases} \tag{1}$$

- f_s : Phase-space distribution function of species s.
- ρ : charge density.
- $\mathbf{E}, \Phi$: electric field and potential.
- $\mathbf{B}$: magnetic field.
- q_s, m_s : charge and mass of a particle of species s.
- ϵ_0 : vacuum permittivity.

PIC methods

- Coupling between Lagrangian method for the Vlasov equation (based on the integration of numerical particle trajectories) and a mesh-based discretization of Poisson's equation for the computation of the self-consistent field.
- f_s represented by a collection of numerical particles with positions and velocities $(\mathbf{x}_p, \mathbf{v}_p)$ which causes a statistical noise $(\mathcal{E}_s)$ **depending on the nb. of particles per cell**.

$$\mathbb{V}(\mathcal{E}_s)^{\frac{1}{2}} \approx \left(\frac{1}{Nh_n^d}\right)^{\frac{1}{2}} \qquad (2)$$

where $h_n = 2^{-n}$ is the grid discretization, d the dimension of the problem and N is the number of particles.

- Coupling between Lagrangian method for the Vlasov equation (based on the integration of numerical particle trajectories) and a mesh-based discretization of Poisson's equation for the computation of the self-consistent field.
- f_s represented by a collection of numerical particles with positions and velocities $(\mathbf{x}_p, \mathbf{v}_p)$ which causes a statistical noise $(\mathcal{E}_s)$ **depending on the nb. of particles per cell**.

$$\mathbb{V}(\mathcal{E}_s)^{\frac{1}{2}} \approx \left(\frac{1}{N h_n^d}\right)^{\frac{1}{2}} \tag{2}$$

where $h_n = 2^{-n}$ is the grid discretization, d the dimension of the problem and N is the number of particles.

PIC scheme

One iteration in time of the scheme consists of:

1. **Scatter**: Accumulate the charge density onto the grid.
2. **Mesh Solver**: Compute the electric field on the grid from the charge density according to Poisson equation:

$$\nabla \cdot \mathbf{E} = \frac{\rho}{\varepsilon_0}, \qquad \mathbf{E} = -\nabla \Phi. \tag{3}$$

3. **Gather**: Interpolate the electric field at particle positions.
4. **Push**: Update the particle positions and velocities from the electric field according to Newton's law:

$$\frac{d\mathbf{x}_p}{dt} = \mathbf{v}_p, \qquad \frac{d\mathbf{v}_p}{dt} = \frac{q_s}{m_s}(\mathbf{E} + \mathbf{v}_p \times \mathbf{B})|_{\mathbf{x}=\mathbf{x}_p}. \tag{4}$$

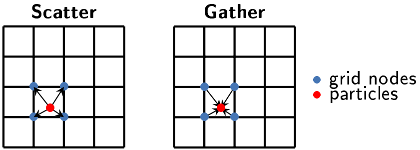

Figure 1: Scatter and gather setps with linear shape functions.

Sparse grids

- A set of coarse anisotropic sparse grids with discretization $h_{\mathbf{l}} = 2^{-\mathbf{l}}$ is considered instead of the regular Cartesian grid, where $\mathbf{l} = (l_1, ..., l_d) \in \mathbb{N}^d$ such that $l_1 + ... + l_d = n + d - 1 - k,\ k \in [\![0, d-1]\!]$.

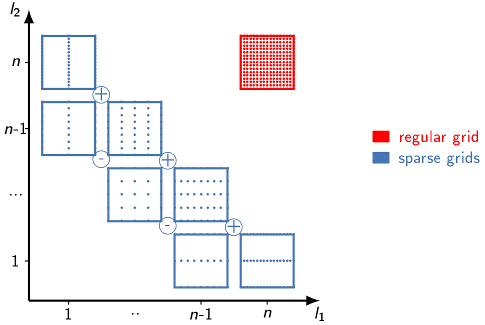

- The set of all sparse grid has $O\left(|\log h_n|^{d-1} h_n^{-1}\right)$ nodes whereas the regular grid has $O\left(h_n^{-d}\right)$ nodes.
- The number of sparse grids considered ranges between 64 and 136 for problems of our iterest (corresponding to a regular grid with 128^3 cells and 1024^3 cells).

Sparse grids

- A set of coarse anisotropic sparse grids with discretization $h_{\mathbf{l}} = 2^{-\mathbf{l}}$ is considered instead of the regular Cartesian grid, where $\mathbf{l} = (l_1, ..., l_d) \in \mathbb{N}^d$ such that $l_1 + ... + l_d = n + d - 1 - k,\ k \in [\![0, d-1]\!]$.

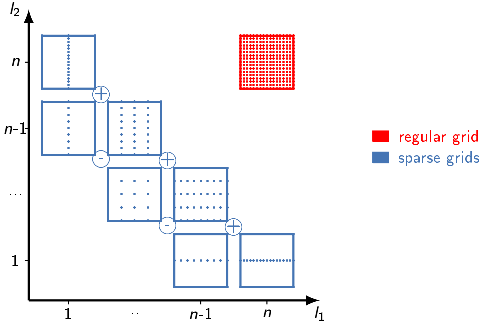

- The set of all sparse grid has $O\left(|\log h_n|^{d-1} h_n^{-1}\right)$ nodes whereas the regular grid has $O\left(h_n^{-d}\right)$ nodes.
- The number of sparse grids considered ranges between 64 and 136 for problems of our iterest (corresponding to a regular grid with 128^3 cells and 1024^3 cells).

One iteration in time of the sparse PIC scheme consists of:

1. **Scatter:** The charge density is accumulated **on each** sparse grid.

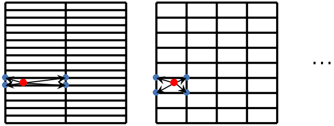

Figure 2: Scatter step on sparse grids with linear shape functions.

2. **Mesh solver:** The electric filed is computed **on each** sparse grid according to Poisson equation:

$$\nabla \cdot \mathbf{E} = \frac{\rho}{\varepsilon_0}, \qquad \mathbf{E} = -\nabla \Phi. \tag{5}$$

3. **Gather:** The electric field is interpolated at particle positions with a linear combination of the electric field of each sparse grid (sparse grid combination technique [2, 4]).
4. **Push:** Similar to standard PIC.

- The method offers a reduction of the statistical noise because sparse grids have larger cells than the regular grid and thus there are more particles per cell.

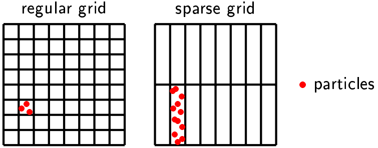

$$\mathbb{V}(\mathcal{E}_s)^{\frac{1}{2}} \lesssim \underbrace{|\log h_n|^{d-1}\left(\frac{1}{Nh_n}\right)^{\frac{1}{2}}}_{\text{sparse}} \leq \underbrace{\left(\frac{1}{Nh_n^d}\right)^{\frac{1}{2}}}_{\text{standard}} \tag{6}$$

- The memory requirements are much lower because of the reduced number of particles for equivalent statistical error.
- The computational cost of the field solver is significantly mitigated because the sparse grids have much less grid nodes than the regular grid.
- A slight additional grid error ($\mathcal{E}_g$) is introduced due to the approximation with the sparse grids [1]:

$$\mathcal{E}_g \approx \underbrace{|\log h_n|^{d-1} h_n^2}_{\text{sparse}} \geq \underbrace{h_n^2}_{\text{standard}} \tag{7}$$

- The method offers a reduction of the statistical noise because sparse grids have larger cells than the regular grid and thus there are more particles per cell.

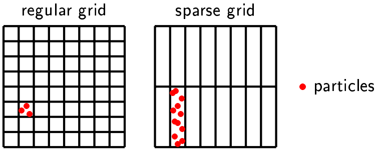

$$\mathbb{V}(\mathcal{E}_s)^{\frac{1}{2}} \lesssim \underbrace{|\log h_n|^{d-1}\left(\frac{1}{Nh_n}\right)^{\frac{1}{2}}}_{\text{sparse}} \leq \underbrace{\left(\frac{1}{Nh_n^d}\right)^{\frac{1}{2}}}_{\text{standard}} \qquad (6)$$

- The memory requirements are much lower because of the reduced number of particles for equivalent statistical error.
- The computational cost of the field solver is significantly mitigated because the sparse grids have much less grid nodes than the regular grid.
- A slight additional grid error ($\mathcal{E}_g$) is introduced due to the approximation with the sparse grids [1]:

$$\mathcal{E}_g \approx \underbrace{|\log h_n|^{d-1} h_n^2}_{\text{sparse}} \geq \underbrace{h_n^2}_{\text{standard}} \qquad (7)$$

3d non linear Landau damping:

- A maxwellian distribution of electrons that are immersed in a uniform, immobile, background of ions is considered.
- Perturbation of a plasma at an equilibrium state.
- Representation of the density at a given time:

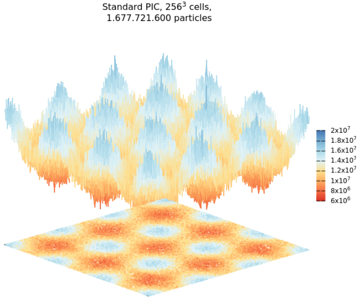

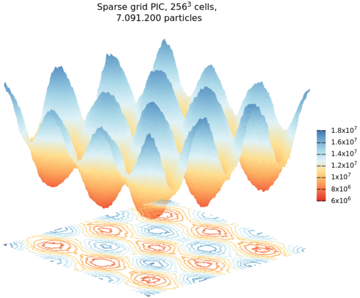

Figure 3: Non linear Landau damping 3d: electron density (2d x-y profile) on a 256^3 grid with 1.6 billion particles and 7 millions (1/225 compared to the std method) for sparse PIC scheme.

- Better statistical resolution with much less particles.

Sequential execution on CPU

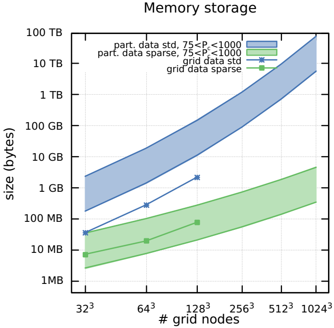

Figure 4: Memory storage (particle, grid, etc.) for the standard and the sparse method.

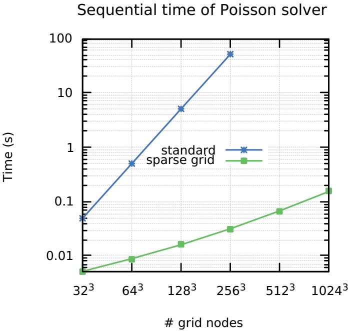

Figure 5: Sequential time of Poisson solver. Multigrid method for standard method, BICGSTAB Jacobi for sparse method. AMD ZEN 3 core.

- The difference between standard and sparse grid methods deepens the more the grid is refined. Thus, demanding problems are more easily achievable...

Simulation on laptop

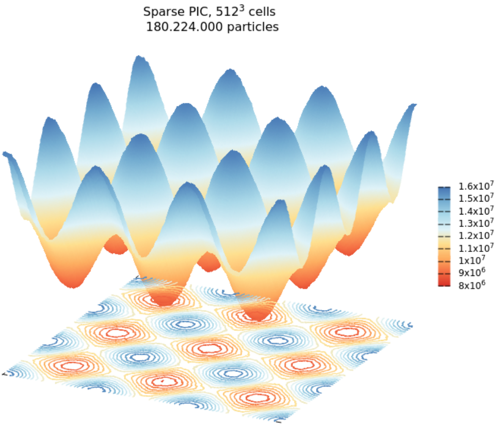

Figure 6: Non linear Landau damping 3d on a 512^3 grid: electron density (2d x-y profile). Simulation on laptop (Intel® Core™ i9-10885H CPU 8 cores @2.40 GHz with 30GB of RAM memory).

- Equivalent to the standard method on a grid with 512^3 cells and 7000 particles per cell (would require roughly 10^{12} particles and 60TB of memory).

Sequential and shared memory parallelism

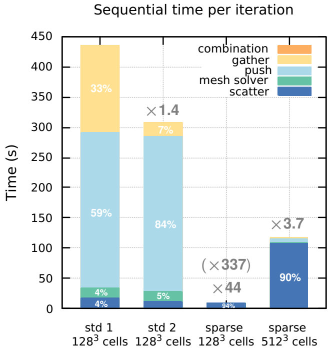

Figure 7: Sequential time for one time iteration (AMD ZEN 3 core).

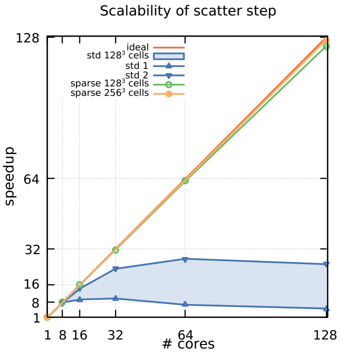

Figure 8: Strong scalability of the scatter step on shared memory NUMA CPUs up to 128 cores (Two CPUs AMD EPYC™ 7713 *Milan*).

- Scatter step takes between 90% and 95% for sparse grid methods (accumulation on all sparse grids).
- Scatter step has a speedup up to 126 on 128 cores with parallelization strategies tailored to sparse grid scheme (future publication).

Acceleration on GPU

- All data fit on the device (single GPU, e.g. Tesla V100 with 16GB memory [3]) for problems up to an equivalent (with respect to standard scheme) of grid with 1024^3 cells and more than 1000 particles per cell.

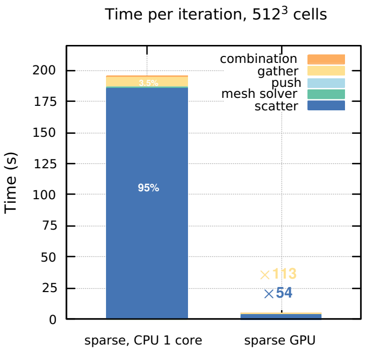

Figure 9: Time per iteration on one CPU Intel® Xeon® Gold 6140 core and Nvidia Tesla V100. Equivalent to 4000 particles per cell.

- It is a work in progress and better acceleration may be expected.

References

F. Deluzet, G. Fubiani, L. Garrigues, C. Guillet, J.Narski, Sparse Grid reconstructions for Particle-In-Cell, in revision.

L. F. Ricketson, A. J. Cerfon, Sparse grid techniques for particle-in-cell schemes, Plasma Physics and Controlled Fusion 59 (2) (2016) 024002.

HPC resources from CALMIP Grant 2022-1125.

M.Griebel, The combination technique for the sparse grid solution of pde's on multiprocessor machines Parallel Process (1992). Lett. 2 61–70.

L. Garrigues, B. Tezenas du Montcel, G. Fubiani, F. Bertomeu, F. Deluzet, and J. Narski. Application of sparse grid combination techniques to low temperature plasmas particle-in-cell simulations. I. Capacitively coupled radio frequency discharges. Journal of Applied Physics, 129(15):153303, April 2021.

L. Garrigues, B. Tezenas du Montcel, G. Fubiani, and B. C. G. Reman. Application of sparse grid combination techniques to low temperature plasmas Particle-In-Cell simulations. II. Electron drift instability in a Hall thruster. Journal of Applied Physics, 129(15):153304, April 2021.

- Application of sparse grid methods to a Hall thruster in 3d (M. Chung-To-Sang) (work in progress).